

Exclusive Measurement of the $\eta \rightarrow \pi^+ \pi^- \gamma$ Decay

The WASA-at-COSY Collaboration

P. Adlarson^a, C. Adolph^b, W. Augustyniak^c, W. Bardan^{d,e,f}, M. Bashkanov^g, T. Bednarski^d, F.S. Bergmann^h, M. Berłowskiⁱ, H. Bhatt^j, K.-T. Brinkmann^k, M. Büscher^{e,f}, H. Calén^a, H. Clement^g, D. Coderre^{e,f,l}, E. Czerwiński^{d,1}, E. Doroshkevich^g, R. Engels^{e,f}, W. Erven^{m,f}, W. Eyrich^b, P. Fedoretsⁿ, K. Föhl^o, K. Fransson^a, F. Goldenbaum^{e,f}, P. Goslawski^h, K. Grigoryev^{e,f,p}, C.-O. Gullström^a, C. Hanhart^{e,f,q}, L. Heijmanskjöld^a, J. Heimlich^b, V. Hejny^{e,f}, F. Hinterberger^k, M. Hodana^{d,e,f}, B. Höistad^a, M. Jacewicz^a, A. Jany^d, B.R. Jany^d, L. Jarczyk^d, T. Johansson^a, B. Kamys^d, G. Kemmerling^{m,f}, O. Khakimova^g, A. Khoukaz^h, S. Kistryn^d, J. Klaja^{d,e,f}, H. Kleines^{m,f}, B. Kłos^r, F. Kren^g, W. Krzemień^d, P. Kulesa^s, A. Kupśca^a, K. Lalwanjⁱ, S. Leupold^a, B. Lorentz^{e,f}, A. Magiera^d, R. Maier^{e,f}, B. Mariański^c, P. Marciniowski^a, U.-G. Meißner^{e,f,q,k,t}, M. Mikirtychiants^{e,f,p}, H.-P. Morsch^c, P. Moskal^d, B.K. Nandjⁱ, S. Niedźwiecki^d, H. Ohm^{e,f}, A. Passfeld^h, C. Pauly^{e,f,2}, E. Perez del Rio^g, T. Petri^{e,f}, Y. Petukhov^u, N. Piskunov^u, P. Pluciński^a, P. Podkopał^d, A. Povtoreyko^u, D. Prasuhn^{e,f}, A. Pricking^g, K. Pysz^s, A. Pyszniak^d, T. Rausmann^h, C.F. Redmer^{a,*}, J. Ritman^{e,f,l}, A. Roy^v, Z. Rudy^d, S. Sawant^l, S. Schadmand^{e,f}, A. Schmidt^b, T. Sefzick^{e,f}, V. Serdyuk^{e,f,w}, N. Shah^j, M. Siemaszko^r, R. Siudak^s, T. Skorodko^g, M. Skurzok^d, J. Smyrski^d, V. Sopovⁿ, R. Stassen^{e,f}, J. Stepaniakⁱ, G. Sterzenbach^{e,f}, H. Stockhorst^{e,f}, F. Stollenwerk^{e,f}, A. Szczurek^s, A. Täschner^h, C. Terschläusen^a, T. Tolba^{e,f,3}, A. Trzciński^c, R. Varma^j, P. Vlasov^k, G.J. Wagner^g, W. Węglorz^r, A. Winnemöller^h, A. Wirzba^{e,f,q}, M. Wolke^a, A. Wrońska^d, P. Wüstner^{m,f}, P. Wurm^{e,f}, X. Yuan^x, L. Yurev^{e,f,w}, J. Zabierowski^y, C. Zheng^x, M.J. Zieliński^d, W. Zipper^r, J. Złomańczuk^a, P. Żuprański^c

^aDivision of Nuclear Physics, Department of Physics and Astronomy, Uppsala University, Box 516, 75120 Uppsala, Sweden

^bPhysikalisches Institut, Friedrich–Alexander–Universität Erlangen–Nürnberg, Erwin–Rommel–Str. 1, 91058 Erlangen, Germany

^cDepartment of Nuclear Reactions, The Andrzej Soltan Institute for Nuclear Studies, ul. Hoza 69, 00-681, Warsaw, Poland

^dInstitute of Physics, Jagiellonian University, ul. Reymonta 4, 30-059 Kraków, Poland

^eInstitut für Kernphysik, Forschungszentrum Jülich, 52425 Jülich, Germany

^fJülich Center for Hadron Physics, Forschungszentrum Jülich, 52425 Jülich, Germany

^gPhysikalisches Institut, Eberhard–Karl–Universität Tübingen, Auf der Morgenstelle 14, 72076 Tübingen, Germany

^hInstitut für Kernphysik, Westfälische Wilhelms–Universität Münster, Wilhelm–Klemm–Str. 9, 48149 Münster, Germany

ⁱHigh Energy Physics Department, The Andrzej Soltan Institute for Nuclear Studies, ul. Hoza 69, 00-681, Warsaw, Poland

^jDepartment of Physics, Indian Institute of Technology Bombay, Powai, Mumbai–400076, Maharashtra, India

^kHelmholtz–Institut für Strahlen– und Kernphysik, Rheinische Friedrich–Wilhelms–Universität Bonn, Nußallee 14–16, 53115 Bonn, Germany

^lInstitut für Experimentalphysik I, Ruhr–Universität Bochum, Universitätsstr. 150, 44780 Bochum, Germany

^mZentralinstitut für Elektronik, Forschungszentrum Jülich, 52425 Jülich, Germany

ⁿInstitute for Theoretical and Experimental Physics, State Scientific Center of the Russian Federation, Bolshaya Cheremushkinskaya 25, 117218 Moscow, Russia

^oII. Physikalisches Institut, Justus–Liebig–Universität Gießen, Heinrich–Buff–Ring 16, 35392 Giessen, Germany

^pHigh Energy Physics Division, Petersburg Nuclear Physics Institute, Orlova Roshka 2, 188300 Gatchina, Russia

^qInstitute for Advanced Simulation, Forschungszentrum Jülich, 52425 Jülich, Germany

^rAugust Chelkowski Institute of Physics, University of Silesia, Uniwersytecka 4, 40-007, Katowice, Poland

^sThe Henryk Niewodniczański Institute of Nuclear Physics, Polish Academy of Sciences, 152 Radzikowskiego St, 31-342 Kraków, Poland

^tBethe Center for Theoretical Physics, Rheinische Friedrich–Wilhelms–Universität Bonn, 53115 Bonn, Germany

^uVeksler and Baldin Laboratory of High Energy Physics, Joint Institute for Nuclear Physics, Joliot–Curie 6, 141980 Dubna, Russia

^vDepartment of Physics, Indian Institute of Technology Indore, Khandwa Road, Indore–452017, Madhya Pradesh, India

^wDzhelepov Laboratory of Nuclear Problems, Joint Institute for Nuclear Physics, Joliot–Curie 6, 141980 Dubna, Russia

^xInstitute of Modern Physics, Chinese Academy of Sciences, 509 Nanchang Rd., 730000 Lanzhou, China

^yDepartment of Cosmic Ray Physics, The Andrzej Soltan Institute for Nuclear Studies, ul. Uniwersytecka 5, 90-950 Lodz, Poland

Abstract

An exclusive measurement of the decay $\eta \rightarrow \pi^+ \pi^- \gamma$ has been performed at the WASA facility at COSY. The η mesons were produced in the fusion reaction $\text{pd} \rightarrow {}^3\text{He} X$ at a proton beam momentum of 1.7 GeV/c. Efficiency corrected differential distributions have been extracted based on 13960 ± 140 events after background subtraction. The measured pion angular distribution is consistent with a relative p -wave of the two-pion system, whereas the measured photon energy spectrum was found at variance with the simplest gauge invariant matrix element of $\eta \rightarrow \pi^+ \pi^- \gamma$. A parameterization of the data can be achieved by the additional inclusion of the empirical pion vector form factor multiplied by a first-order polynomial in the squared invariant mass of the $\pi^+ \pi^-$ system.

Keywords: η meson, box anomaly, exclusive measurement

PACS: 14.40.Be, 13.20.Jf, 12.39.Fe

arXiv:1107.5277v2 [nucl-ex] 17 Nov 2011

1. Introduction

The η meson plays a special role in understanding low-energy Quantum Chromo Dynamics (QCD). Chiral symmetry, its realization in hadron physics at low energies and the role of explicit chiral symmetry breaking due to the masses of the light quarks (u, d, s) can be investigated using η decays. This work focuses on the anomalous sector of QCD, which is manifested in the radiative decays of the η meson.

The radiative decay $\eta \rightarrow \pi^+\pi^-\gamma$ is the fourth strongest decay mode of the η meson with a branching ratio of $4.60 \pm 0.16\%$ [1]. Conservation of charge conjugation and angular momentum including parity constrain the dynamics of the decay products. The photon and the η meson are eigenstates of the charge symmetry transformation with the eigenvalues $C = -1$ and $C = +1$, respectively. Therefore, due to C invariance the $\pi^+\pi^-$ system must have $C = -1$. To ensure C invariance, the orbital angular momentum L between the two pions must be odd. All involved particles have negative parity. Consequently, parity invariance demands that the orbital angular momentum L' between the photon and the two-pion system must also be odd. Finally, total angular momentum conservation incorporating the fact that the intrinsic spin of the photon is unity leads to the requirement $L = L'$. Thus, the lowest partial waves which contribute are p -waves. Presumably, higher partial waves with $L \geq 3$ are not very important.

Radiative decays of the η meson are driven by the chiral anomaly of QCD. The effects of the anomaly have been summarized by Wess and Zumino in an effective Lagrangian [2]. As shown by Witten, this Lagrangian is an essential part of effective field theories, because it is necessary in order to correctly incorporate the parity transformation of QCD [3]. At the chiral limit of zero momentum and massless quarks the decay $\eta \rightarrow \pi^+\pi^-\gamma$ is determined by the box anomaly term of the Wess-Zumino-Witten Lagrangian, which describes the direct coupling of three pseudoscalar mesons and a photon. The dynamic range of the decay is limited by two pion rest masses and the η mass, $4m_\pi^2 \leq s_{\pi\pi} \leq m_\eta^2$, and is, thus, far from the chiral limit. As a consequence, the decay rate calculated from the box anomaly term at the tree level is smaller by a factor of two compared to the measured value. Higher order terms of the chiral Lagrangian have to be taken into account to achieve a correct description of the decay $\eta \rightarrow \pi^+\pi^-\gamma$. Calculations at the one-loop level show an improved agreement between experiment and theory [4]. But there remains, however, a significant difference. Several efforts have been made to include final state interactions by unitarized extensions to the box-anomaly term, e.g. a momentum dependent Vector Meson Dominance (VMD)

model [5], the Hidden Local Symmetry model [6], an Omnès-function which accounts for the p -wave pion scattering phase shift [7, 8], and a Chiral Unitary approach [9].

To test the validity of the different models, not only the decay rate but also differential distributions of the Dalitz plot variables need to be compared with experimental data. For this purpose it is useful to parameterize the Dalitz plot in terms of the photon energy E_γ in the rest frame of the η meson and the angle θ of the π^+ relative to the photon in the pion-pion rest frame. E_γ is related to the squared invariant mass of the pion pair $s_{\pi\pi}$ according to

$$E_\gamma = \frac{1}{2} \left(m_\eta - \frac{s_{\pi\pi}}{m_\eta} \right). \quad (1)$$

The photon energy distribution has been subject of only a few measurements forty years ago [10, 11, 12, 13]. The results of the two statistically most significant publications [12, 13] are presented without acceptance corrections. Instead, the models which have been used for the interpretation of the data were folded with the acceptance and the results seem to be inconsistent [6, 14].

Due to the limitations of the currently available experimental data the potential of the decay $\eta \rightarrow \pi^+\pi^-\gamma$ to provide insight to the anomalous sector of QCD cannot be fully exploited. In order to perform compelling tests of the box anomaly and its higher order terms in Chiral Perturbation Theory as well as of the non-perturbative extensions of the box-anomaly terms a new measurement with higher precision is called for.

2. The Experiment

The results presented in this paper are based on a measurement with the WASA detection system [15] installed at the Cooler Synchrotron COSY [16] at the Forschungszentrum Jülich in Germany. A pellet target system produces small spheres of frozen hydrogen or deuterium which interact with the ion beam of the accelerator. The interaction region is surrounded by a central detector covering scattering angles from 20 to 169 degrees. It consists of a straw tube drift chamber, which is operated in the magnetic field of 0.85 T provided by a superconducting solenoid for the momentum reconstruction of charged particles, an electromagnetic calorimeter to measure energies of charged as well as neutral particles and thin plastic scintillators to discriminate charged and neutral particles already at the trigger level. Energy loss patterns in the calorimeter and the plastic scintillators allow to identify charged particles. For the identification and reconstruction of particles emitted at polar angles from 3 to 18 degrees a forward detector is used. While track coordinates are measured precisely by a straw tube drift chamber, the kinetic energies of the ejectiles are reconstructed from the signals in plastic scintillators of different thickness, using the ΔE -E method.

The η mesons have been produced in the fusion reaction $pd \rightarrow {}^3\text{He} X$ at a proton beam momentum of 1.7 GeV/c. This corresponds to an excess energy of 60 MeV in the center of mass for the reaction $pd \rightarrow {}^3\text{He} \eta$ at a cross section of

*Corresponding author

Email address: christoph.redmer@physics.uu.se (C.F. Redmer)

¹present address: INFN, Laboratori Nazionali di Frascati, Via E. Fermi 40, 00044 Frascati (Roma), Italy

²present address: Fachbereich Physik, Bergische Universität Wuppertal, Gaußstr. 20, 42119 Wuppertal, Germany

³present address: Albert Einstein Center for Fundamental Physics, Fachbereich Physik und Astronomie, Universität Bern, Sidlerstr. 5, 3012 Bern, Switzerland

0.412 μb [17]. At the trigger level events with one track in the forward detector with a high energy deposit in the thin scintillator detectors close to the exit window of the scattering chamber have been accepted. This condition selects ${}^3\text{He}$ ions without bias on the η decay system.

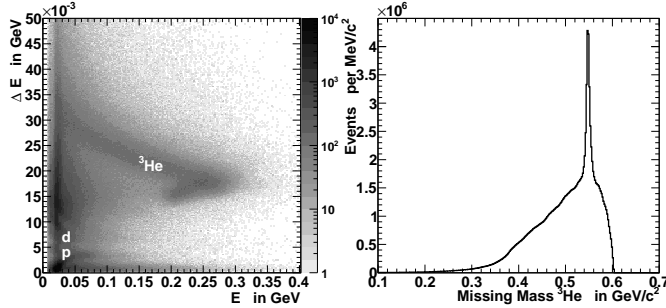


Figure 1: (Left) ΔE - E plot for tracks emitted at scattering angles between 3 and 18 degree. ${}^3\text{He}$ is well separated from protons and deuterons. (Right) Missing mass of ${}^3\text{He}$ for all events in the ${}^3\text{He}$ band. The number of events in the peak above the background is $1.1 \cdot 10^7$.

Fig. 1 shows the energy loss correlations of all tracks in the forward detector. The structure attributed to ${}^3\text{He}$ is clearly visible and can be easily selected. It is well separated from the structures of protons and deuterons, which are strongly suppressed due to the trigger conditions. The right panel of Fig. 1 shows the inclusive missing mass distribution of ${}^3\text{He}$. A pronounced peak at the η meson mass is visible. It contains $1.1 \cdot 10^7$ tagged mesons on top of a continuous background which originates from direct multi-pion production. The cross sections of the relevant background processes $pd \rightarrow {}^3\text{He} \pi^+ \pi^-$ and $pd \rightarrow {}^3\text{He} \pi^+ \pi^- \pi^0$ are unknown at the center-of-mass energy of this measurement. However, they can be estimated, by extrapolation of results at lower energies [18], to be about $5 \mu\text{b}$ and $0.4 \mu\text{b}$, respectively. The missing mass spectrum in the right panel of Fig. 1 illustrates that the direct reactions contribute to the background for η decays only in a range of a few MeV/c^2 around the η meson mass. This remaining background is subtracted in a model independent way, bin by bin from the final spectra.

3. Data Analysis

For the selection of the final state, one charged particle, which is identified as ${}^3\text{He}$, is required in the forward detector. In the central detector, two charged particle tracks of opposite curvature and one neutral particle track with an energy deposit in the calorimeter of at least 20 MeV are required in addition. Both charged particles are identified as pions. Background events which are picked up by the selection rules stem mainly from charged multi-pion production and other η decay modes.

Two-pion production is expected to form the largest background contribution in the selected data due to the large cross section and the possibility of cluster splitoffs in the calorimeter, which would fake the signal of a photon candidate in the

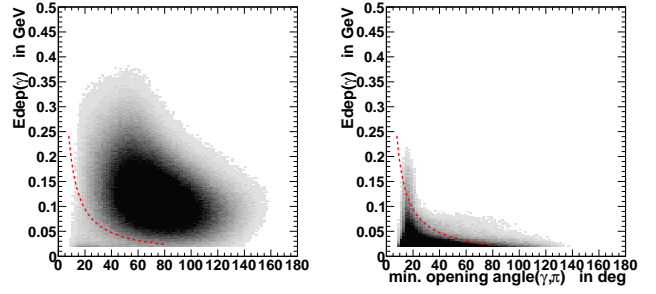


Figure 2: Correlation plot for laboratory photon energy vs charged track photon opening angle (Monte Carlo) (left): signal, (right): $pd \rightarrow {}^3\text{He} \pi^+ \pi^-$ reaction. The graphical cut to suppress $pd \rightarrow {}^3\text{He} \pi^+ \pi^-$ reaction is shown.

actually photon free final state. Splitoffs are characterized by a small energy deposit and a small distance to either of the pion candidates in the calorimeter. Therefore, this background contributes predominantly to the low end of the reconstructed E_γ spectrum. In order to increase the signal to background ratio in this region a correlated condition is imposed on the energy deposits of the photon candidates and the distance between the shower positions of photon and pion candidates in the calorimeter. The latter is measured by the opening angle between the reconstructed cluster positions. In Fig. 2 the condition is shown as graphical cut with a dashed curve. A strong enhancement is observed at low photon energies and small opening angles between photon and pion candidates from the contribution of the $pd \rightarrow {}^3\text{He} \pi^+ \pi^-$ reaction. The cut used is the best compromise between a high signal-to-background ratio and a large reconstruction efficiency of the signal channel. The contribution from two-pion production is reduced by more than 55% by rejecting all events below the curve.

Final states with three pions contribute to the background only if one photon of the π^0 decay remains undetected. The π^0 can be identified from the distribution of the squared missing mass of the ${}^3\text{He} \pi^+ \pi^-$ system, as demonstrated in Fig. 3. Here, the experimental missing mass spectrum is reproduced with Monte Carlo distributions of the the signal ($\eta \rightarrow \pi^+ \pi^- \gamma$) and background ($\eta \rightarrow \pi^+ \pi^- \pi^0, \eta \rightarrow e^+ e^- \gamma$) contributions from η decays as well as direct two- and three-pion production. The cross sections of the direct pion processes were fitted using simultaneously the ${}^3\text{He} \pi^+ \pi^-$ missing mass distribution and the ${}^3\text{He}$ missing mass for the selected data sample. The result is in agreement with the expectations [18]. The contributions of the different η meson decay channels are fixed by the known branching ratios [1]. The discrepancy between Monte Carlo and experiment for negative masses might be attributed to the unknown production mechanisms of the direct processes. In the simulations isotropic phase space population has been assumed. The discrepancy disappears when the contribution of the direct production is subtracted bin-by-bin, as discussed later. By rejecting events with a squared missing mass value larger than $0.0125 \text{ GeV}^2/c^4$, as indicated with a vertical dashed line in Fig. 3, 73% of the background from the ${}^3\text{He} \pi^+ \pi^- \pi^0$ final states in the mass region of the η meson is removed.

Additional suppression of background is achieved by a kine-

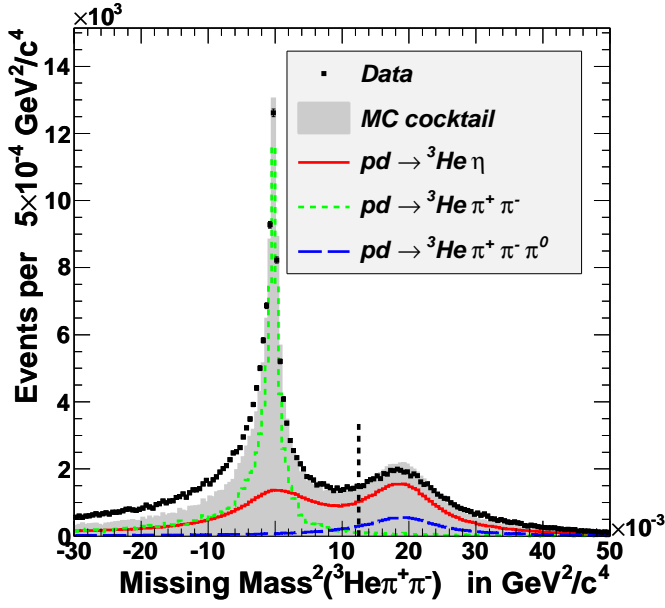


Figure 3: The π^0 signal in the squared missing mass of the ${}^3\text{He} \pi^+ \pi^-$ system. The dashed vertical line corresponds to a squared missing mass of $0.0125 \text{ GeV}^2/c^4$.

matic fit of the complete final state to the reaction hypothesis $pd \rightarrow {}^3\text{He} \pi^+ \pi^- \gamma$, using four-momentum conservation as the only fit constraint. The uncertainties of the kinematic variables at the input to the fit have been extracted depending on energy and angle from a GEANT Monte Carlo simulation, tuned to match the experimental resolutions. After the fit, all events with a probability of less than 10% are rejected. The invariant mass distribution of the fitted $\pi^+ \pi^- \gamma$ system is shown for the remaining events in Fig. 4. The condition on the probability distribution additionally suppresses background. In particular a comparison with Monte Carlo shows a reduction of the ${}^3\text{He} \pi^+ \pi^- \pi^0$ background to the level of 10% in the selected events.

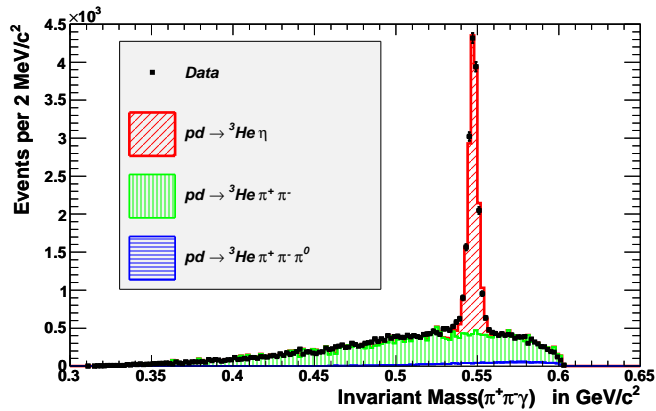


Figure 4: The invariant mass spectrum of the fitted $\pi^+ \pi^- \gamma$ system with a probability above 10%. The Monte Carlo cocktail consists of the signal ($\eta \rightarrow \pi^+ \pi^- \gamma$) and background contributions ($\eta \rightarrow \pi^+ \pi^- \pi^0$, $\eta \rightarrow e^+ e^- \gamma$) from η decays (diagonally hatched) as well as direct two-pion (vertically hatched) and three-pion (horizontally hatched) production.

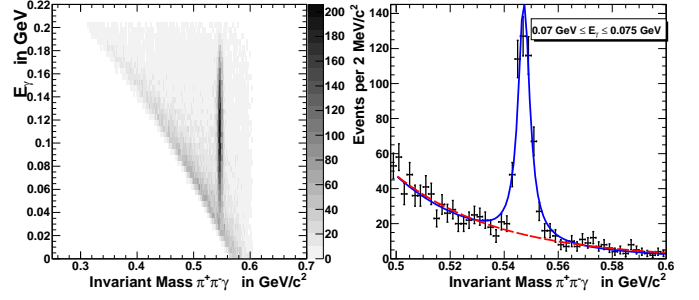


Figure 5: Background subtraction from the E_γ distribution. **Left:** Correlation of E_γ and the invariant mass of the $\pi^+ \pi^- \gamma$ system. **Right:** Illustration of the background subtraction methods with the invariant mass spectrum corresponding to the photon energy region $70 \leq E_\gamma [\text{MeV}] \leq 75$: Determination of the background shape by fitting signal and background (solid curve) and by excluding the signal range from the fit of the background (dashed curve).

The remaining background is subtracted bin by bin from the E_γ and $\cos \theta$ distributions. The bin size of 5 MeV for the photon energy and 0.1 for the pion angular distributions is chosen to reflect the resolution achieved in the respective observables. The bin width of the angular distribution is similar to previous measurements [12, 13] the bin width of the E_γ spectrum is smaller by about a factor of two. The left panel in Fig. 5 shows the correlation between the photon energy and the invariant mass of the $\pi^+ \pi^- \gamma$ system. Two structures can be seen in the plot. One at the mass of the η meson containing the signal events and another structure, showing a correlation of photon energy and invariant mass, caused mainly by background from two-pion production. The invariant mass of the $\pi^+ \pi^- \gamma$ system is calculated for the events in each bin of the E_γ and $\cos \theta$ distributions. This is illustrated for one bin of the E_γ distribution in the right panel of Fig. 5. Since both, cross sections and differential distributions are unknown for multi-pion production at the energy of this measurement, the individual mass spectra are fitted in two ways in order to determine the amount of continuous background in the η mass region. In the first approach a function that is the sum of a Lorentzian for the signal and an exponential for the background is used. In the second method the background is fitted with an exponential function without making an assumption on the signal shape by excluding the range of the signal peak from the fit. The excluded region was determined as the 3σ region of a Gaussian fit to the peak of the η meson. The individual results of the fits using both methods are shown in the right panel of Fig. 5 with solid and dashed curves, respectively. The average number of the background events from both fits is used to calculate the number of events from the η meson decay in the corresponding bin of the E_γ or $\cos \theta$ distribution.

The remaining background from the $\eta \rightarrow \pi^+ \pi^- \pi^0$ decay in the signal region is subtracted using scaled Monte Carlo distributions. The scaling factors are determined by a fit of the experimental spectrum of the squared missing mass of the ${}^3\text{He} \pi^+ \pi^-$ system with Monte Carlo distributions of the relevant η decay modes, $\eta \rightarrow \pi^+ \pi^- \gamma$ (signal), $\eta \rightarrow \pi^+ \pi^- \pi^0$ and $\eta \rightarrow e^+ e^- \gamma$ (background), after subtraction of the continuous background from multi-pion production. The contribution of $\eta \rightarrow \pi^+ \pi^- \pi^0$

determined to be 7%. This background is isotropic in $\cos\theta$ and contributes to the E_γ distribution in the energy region above 50 MeV with a maximum at 120 MeV. The total statistics in the final distributions is 13960 ± 140 events of the $\eta \rightarrow \pi^+\pi^-\gamma$ decay. This is the largest number of events from an exclusive measurement of this decay mode.

For acceptance corrections the general form of the squared matrix element for the $\eta \rightarrow \pi^+\pi^-\gamma$ decay

$$|\mathcal{M}|^2 \sim |F(s_{\pi\pi})|^2 E_\gamma^2 q^2 \sin^2(\theta) \quad , \quad (2)$$

with q being the pion momentum in the pion-pion rest frame, and the form factor $F(s_{\pi\pi})$ according to the VMD calculations in Ref. [5] has been used. Using instead Monte Carlo distributions based on the simplest gauge invariant matrix element ($F(s_{\pi\pi}) = \text{const.}$) does not alter the experimental result significantly. Thus, it can be concluded that systematic effects due to the applied form factors are negligible. The acceptance varies smoothly as a function of E_γ and $\cos\theta$. For photon energies less than 10 MeV the acceptance becomes vanishingly small. In case of the angular distribution a reduced acceptance is observed for small opening angles between each of the pions and the photon. The reduction of the acceptance in both variables is found to be correlated. It is caused by the method of two-pion suppression presented in Fig. 3, where a condition on the correlation of photon energy and opening angle between pion and photon candidates is used.

4. Results

Fig. 6 shows the background subtracted and acceptance corrected photon energy and pion angular distributions with the statistical errors. The E_γ distribution is also given numerically in Tab. 2.

In the upper panel of Fig. 6 the final distribution of $\cos\theta$ is shown. It can be described by $d\sigma/d\cos\theta = A \cdot \sin^2(\theta)$, as indicated by the dashed curve. Thus, the measurement is consistent with the relative p -wave assumed in Eq. 2.

The photon energy distribution in the η rest frame is shown in the lower panel of Fig. 6. The line shape obtained from Eq. 2, normalized to the integrated rate, is given by the dashed curve. It does not describe the experimental data, which in comparison are shifted significantly towards lower energies. The observed disagreement confirms the findings of the previous measurements [10, 11, 12, 13].

In order to achieve a correct description of the photon energy spectrum in addition to the already properly described angular distribution, Eq. 2 can be multiplied by an energy dependent form factor $|FF(s_{\pi\pi})|^2$. The origin of the deviation in the E_γ distribution is predominantly given by the $\pi\pi$ final state interaction in the vector channel. Unitarity and analyticity dictate that this effect should be given by the pion vector form factor $F_V(s_{\pi\pi})$ multiplied by a polynomial $P(s_{\pi\pi})$ that parameterizes contributions that do not contain the $\pi\pi$ unitarity cut. For a detailed discussion about the multiplier $|FF(s_{\pi\pi})|^2 = |F_V(s_{\pi\pi})P(s_{\pi\pi})|^2$ of Eq. 2 see *e.g.* Refs. [7, 8, 19, 20]. The pion vector form factor is experimentally directly accessible via $e^+e^- \rightarrow \pi^+\pi^-$ or may

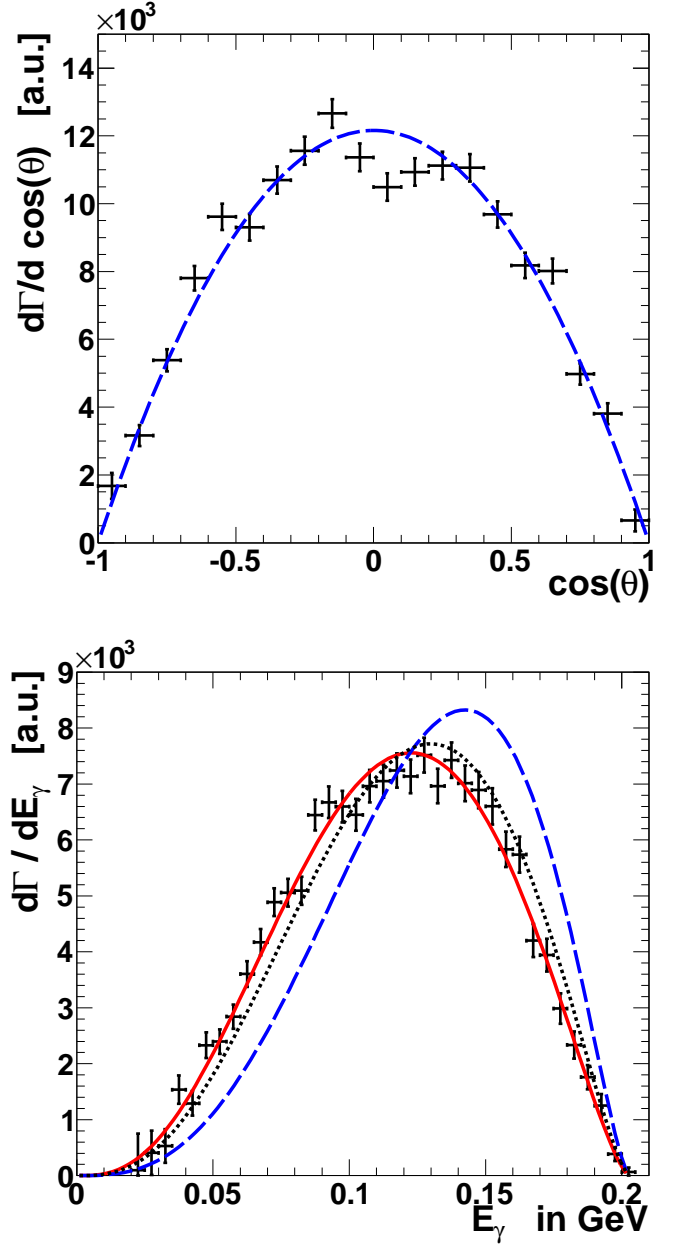


Figure 6: The background subtracted and acceptance corrected angular distribution of the pions (top) and the photon energy distribution (bottom), with error bars indicating the statistical uncertainties. The angular distribution is compared with a relative p -wave of the pions (dashed curve). The shape of the photon energy distribution is confronted with predictions of the square of the simplest gauge invariant matrix element, Eq. 2 (dashed curve), multiplied by the squared modulus of the pion vector form factor $|F_V(s_{\pi\pi})|^2$ (dotted curve) and further multiplied by $(1 + \alpha s_{\pi\pi})^2$, the square of a real polynomial of first order, with its coefficient fitted to the data (solid curve). All curves are normalized to the same integral.

be derived using the Omnes representation from the $\pi\pi$ elastic phase shifts in the vector channel — here the representation for $F_V(m_{\pi\pi})$ derived in Ref. [20, 22] is applied. The uncertainty in this form factor is negligible compared to the experimental uncertainties, which are presented in detail in the next paragraph. Furthermore, following Refs. [7, 8, 20], we parameterize the

term $P(s_{\pi\pi})$ as a real polynomial of first order:

$$P(s_{\pi\pi}) = 1 + \alpha s_{\pi\pi}. \quad (3)$$

The parameter α can then be determined from a fit to the data, which is shown with the solid curve in the lower panel of Fig. 6. The result for $\alpha = 0$ is shown as the dotted curve.

Tests for systematic uncertainties of α have been performed by varying in the analysis chain one by one the conditions for the suppression of splitoffs, the cut on the missing mass of the ${}^3\text{He}\pi^+\pi^-$ system, the condition on the probability of the kinematic fit, the method of subtracting the background from direct multi-pion production, the $\eta \rightarrow \pi^+\pi^-\pi^0$ contribution and the model used for the acceptance correction. Additionally, subsets of the data, collected with different experimental settings, allowed to cross check the influences of luminosity variations and different RF settings during the measurement.

Using different methods to subtract the continuous multi-pion background, different models to perform the acceptance correction or using different RF settings does not cause statistically significant deviations from the original result. The contributions to the systematic uncertainty of α derived from the other tests are listed in Tab. 1. The overall systematic error is obtained by adding the contributions quadratically.

One of the largest uncertainties results from the fluctuations of the luminosity during data taking. The variation of the final result with the chosen luminosity can be explained by the accuracy of the simulations concerning pile-up effects and beam-target overlap parameters, which have not been included in a systematic way.

Test	σ
Splitoffs	0.34
MM($\text{He}\pi^+\pi^-$) cut	0.22
$P(\chi_{kf}^2, \text{ndf})$	0.12
$\eta \rightarrow \pi^+\pi^-\pi^0$ bkg.	0.26
Luminosity effects	0.32

Table 1: Summary of contributions to the systematic uncertainty of the parameter α .

Taking into account the systematic studies, the final result for the parameter α is:

$$\alpha = 1.89 \pm 0.25_{\text{stat}} \pm 0.59_{\text{sys}} \pm 0.02_{\text{theo}} \text{ GeV}^{-2},$$

where the theoretical uncertainty results from the uncertainty of the pion vector form factor due to the input of Ref. [21] for the $\pi\pi$ phase shifts and the extrapolation beyond the upper cutoff. For more details, see Ref. [20].

In comparison to theory, calculations based on vector meson dominance [5, 6] result in a shape of the differential distribution corresponding to an $\alpha = (0.23 \pm 0.01) \text{ GeV}^{-2}$. The shape given by a parameterization of the pion vector form factor combined with a fit to vector meson dominance [7, 8] corresponds to an $\alpha = (0.64 \pm 0.02) \text{ GeV}^{-2}$. The E_γ spectrum from one-loop Chiral Perturbation Theory [4] can be described with an

$\alpha = -(0.7 \pm 0.1) \text{ GeV}^{-2}$. Thus, the available theory descriptions produce distributions of E_γ , which are close to the curve of $\alpha = 0$ shown with a dotted line in the right panel of Fig. 6. Within the total error of the measurement, the value of α found in this work appears to be only compatible with the works of Refs. [7, 8].

E_γ [GeV]	Entries [a.u.]	stat. [a.u.]
0.0225	97	653
0.0275	407	394
0.0325	530	302
0.0375	1537	252
0.0425	1291	220
0.0475	2331	227
0.0525	2397	218
0.0575	2841	217
0.0625	3604	228
0.0675	4171	235
0.0725	4887	247
0.0775	5057	248
0.0825	5091	252
0.0875	6444	273
0.0925	6673	282
0.0975	6595	282
0.1025	6448	284
0.1075	6961	291
0.1125	7051	297
0.1175	7242	304
0.1225	7138	300
0.1275	7514	312
0.1325	6963	309
0.1375	7425	317
0.1425	7014	319
0.1475	6892	323
0.1525	6600	324
0.1575	5833	315
0.1625	5739	320
0.1675	4200	294
0.1725	3942	292
0.1775	2985	270
0.1825	2334	244
0.1875	1760	217
0.1925	1250	207
0.1975	384	125
0.2025	63	79

Table 2: Distribution of the photon energy in the η rest frame with statistical errors. The values of E_γ are central values of bins with a width of 5 MeV.

5. Conclusions

For the first time, background subtracted and acceptance corrected differential distributions of the decay $\eta \rightarrow \pi^+\pi^-\gamma$ have been extracted in the analysis of exclusive data. The distributions clearly show the importance of final state interactions. The shape of the E_γ spectrum can be very well described by a parameterization that includes the factors required by gauge invariance and the centrifugal barrier as well as the pion vector form factor times a first-order

polynomial written as $(1 + \alpha s_{\pi\pi})$. A fit to the data gives $\alpha = 1.89 \pm 0.25_{stat} \pm 0.59_{sys} \pm 0.02_{theo} \text{ GeV}^{-2}$. In order to shed further light on the anomalous sector of QCD, future theoretical studies will have to explain simultaneously both the value of α as well as the branching ratio for $\eta \rightarrow \pi^+\pi^-\gamma$.

In recent production runs of the WASA facility at COSY further data on η decays have been taken with high statistics. From a preliminary analysis at least an order of magnitude more fully reconstructed $\eta \rightarrow \pi^+\pi^-\gamma$ events is expected. The analysis of the acquired data will significantly decrease not only the statistical but also the systematic uncertainties by an improved understanding of background contributions.

The data will also be used to determine the branching ratio of the decay $\eta \rightarrow \pi^+\pi^-\gamma$. A recent measurement of the CLEO collaboration [23] shows a relative branching ratio which differs by more than three standard deviations from the results of previous measurements [12, 24]. Due to the unbiased tagging of η mesons in the reaction $pd \rightarrow {}^3\text{He} \eta$ it is not only possible to extract relative but also absolute branching ratios at the WASA facility. This will help to resolve the discrepancy.

6. Acknowledgments

We thank F.-K. Guo for providing us with the code to calculate the pion vector form factor.

This work was in part supported by: the Forschungszentrum Jülich including the JCHP-FFE program, the European Commission under the 7th Framework Programme through the 'Research Infrastructures' action of the 'Capacities' Programme. Call: FP7-INFRASTRUCTURES-2008-1, Grant Agreement N. 227431, the German BMBF, the German-Indian DAAD-DST exchange program, VIQCD (VH-VI-231), the German Research Foundation (DFG), and the Polish National Science Centre and Foundation for Polish Science - MPD program, co-financed by the European Union within the European Regional Development Fund.

We gratefully acknowledge the financial support given by the Knut and Alice Wallenberg Foundation, the Swedish Research Council, the Göran Gustafsson Foundation, the Polish Ministry of Science and Higher Education under the grant PBS 7P-P6-2/07.

We also want to thank the technical and administrative staff at the Forschungszentrum Jülich, especially at the Cooler SYNchrotron COSY and at the participating institutes.

This work is part of the PhD Thesis of C. F. Redmer.

References

- [1] **Particle Data Group** Collaboration, K. Nakamura *J. Phys.* **G37** (2010) 075021.
- [2] J. Wess and B. Zumino *Phys. Lett.* **B37** (1971) 95.
- [3] E. Witten *Nucl. Phys.* **B223** (1983) 422–432.
- [4] J. Bijnens, A. Bramon, and F. Cornet *Phys. Lett.* **B237** (1990) 488.
- [5] C. Picciotto *Phys. Rev.* **D45** (1992) 1569–1574.
- [6] M. Benayoun, P. David, L. DelBuono, P. Leruste, and H. B. O’Connell *Eur. Phys. J.* **C31** (2003) 525–547, [arXiv:nuc1-th/0306078](#).
- [7] E. P. Venugopal and B. R. Holstein *Phys. Rev.* **D57** (1998) 4397–4402, [arXiv:hep-ph/9710382](#).
- [8] B. R. Holstein *Phys. Scripta* **T99** (2002) 55–67, [arXiv:hep-ph/0112150](#).
- [9] B. Borasoy and R. Nisßler *Nucl. Phys.* **A740** (2004) 362–382, [arXiv:hep-ph/0405039](#).
- [10] F. S. Crawford and L. R. Price *Phys. Rev. Lett.* **16** (1966) 333.
- [11] A. M. Cnops *et al. Phys. Lett.* **26B** (1968) 398.
- [12] M. Gormley *et al. Phys. Rev.* **D2** (1970) 501–505.
- [13] J. G. Layter *et al. Phys. Rev.* **D7** (1973) 2565–2568.
- [14] B. Borasoy and R. Nisßler *Eur. Phys. J.* **A33** (2007) 95–106, [arXiv:0705.0954 \[hep-ph\]](#).
- [15] **WASA-at-COSY** Collaboration, H. H. Adam *et al.* [arXiv:nuc1-ex/0411038](#)
- [16] R. Maier *Nucl. Instrum. Meth.* **A390** (1997) 1–8.
- [17] R. Bilger *et al. Phys. Rev.* **C65** (2002) 044608.
- [18] M. Bashkanov *et al. Phys. Lett.* **B637** (2006) 223–228 [arXiv:nuc1-ex/050811](#).
- [19] T. N. Truong *Phys. Rev.* **D65** (2002) 056004, [arXiv:hep-ph/0105123 \[hep-ph\]](#).
- [20] F. Stollenwerk *et al.*, [arXiv:1108.2419v2 \[nucl-th\]](#).
- [21] R. Garcia-Martin *et al.*, *Phys. Rev.* **D83** (2011) 074004.
- [22] F.-K. Guo, C. Hanhart, F. J. Llanes-Estrada, and U.-G. Meißner *Phys. Lett.* **B678** (2009) 90–96, [arXiv:0812.3270 \[hep-ph\]](#).
- [23] **CLEO** Collaboration, A. Lopez *et al. Phys. Rev. Lett.* **99** (2007) 122001, [arXiv:0707.1601 \[hep-ex\]](#).
- [24] J. J. Thaler, J. A. Appel, A. Kotlewski, J. G. Layter, W. Lee, and S. Stein *Phys. Rev.* **D7** (1973) 2569–2571.